International Journal of Microwave and Wireless Technologies

cambridge.org/mrf

2D leaky-wave antenna with controlled direction of radiation in the azimuthal plane

Jan Machac, Milan Svanda and Vaclav Kabourek

Faculty of Electrical Engineering, Czech Technical University in Prague, Prague, Czech Republic

Research Paper

Cite this article: Machac J, Svanda M, Kabourek V (2024) 2D leaky-wave antenna with controlled direction of radiation in the azimuthal plane. *International Journal of Microwave and Wireless Technologies* **16**(7), 1187–1197. https://doi.org/10.1017/S1759078724000448

Received: 22 September 2023
Revised: 15 March 2024
Accepted: 21 March 2024

Keywords:
2D antenna matrix; beam steering; leaky-wave antenna; metasurface; mushroom cells

Corresponding author: Jan Machac; Email: machac@fel.cvut.cz

Abstract

This paper presents a two-dimensional (2D) metasurface antenna array composed of mushroom cells coupled by thin slots in the top metallization. The antenna is fed through power dividers designed in substrate-integrated waveguide technology. The antenna structure is therefore designed in a fully up-to-date integrated version. The array shows beam steering in the azimuthal plane controlled by signal amplitudes fed into particular ports at the edges of the matrix. The main advantage of this antenna is no need to use phase shifters applied in standard 2D antenna arrays. Two antenna versions have been designed, fabricated, and experimentally tested. The beam can be steered within 360° (90°) in azimuth. The steering of the beam in elevation from backward to forward directions within 40° is done by changing frequency from 21 up to 23.8 GHz. This interval is reduced to 30° by exciting the antenna simultaneously at two adjacent ports at the same amplitude.

Introduction

Leaky-wave antennas (LWAs) can be designed as composite right/left-handed (CRLH) periodic structures [1, 2]. Two-dimensional (2D) structures show a great variety of radiation patterns, depending on how they are fed. A structure with central feeding offers a conical radiation pattern [3]. An LWA in the shape of a circular metallic grating excited by a planar launcher has been designed in paper [4]. The structure exhibits conical-sector beam scanning. A 2D LWA based on a CRLH transmission line working in the frequency band from 76 up to 81 GHz has been presented in paper [5]. The structure enables steering the narrow beam in elevation by changing frequency in a hemisphere from −10° to 10° and from −28° to 23°. Recent developments in the area of analyzing 2D LWAs have been presented in paper [6].

A paper cited in paper [7] presents a 2D CRLH metamaterial with an orthogonal feeding structure. This structure is composed of mushroom unit cells coupled mutually by capacitors. By varying the magnitude of the input power to two orthogonal edges of the metamaterial, the net power flow direction can be controlled based on wave interaction, so that the beam is steered in the azimuthal plane. Feeding of particular lines on edges of the antenna matrix is implemented by transitions to 50 Ω microstrip transmission lines.

An optical phased array (OPA) presented in paper [8] was composed of N × N radiating elements and fed by a 1502 nm laser. The number of phase shifters has been reduced from N^2 to 2N (similarly as in a peripherally excited phased array proposed in paper [9]). This OPA is able to steer the beam in the azimuthal plane within 360°. A peripherally excited array [9] is able to steer the beam within in elevation from −33° to 33° and depending on the excited side in azimuthal sectors again from −33° to 33°. Paper [10] presents an LWA antenna based on array of CRLH transmission lines. These lines are fed through series power divider feeding an entire system of phase shifters assuring scanning in azimuth connected to mixers assuring frequency steering in elevation. The structure offers the full-space scanning. The complexity of this antenna is in the application of phase shifters and mixers assuring frequency scanning. A fixed-frequency 2D single-fed reconfigurable Fabry–Perot antenna has been proposed to electronically steer a pencil beam in both azimuthal and elevation planes in paper [11]. The antenna is based on a tunable high impedance surface with varactors divided into four independently biased sectors, so that a sectorized Fabry–Perot antenna topology is obtained. Each azimuthal sector is tuned into the electromagnetic bandgap dispersion region, so that the pencil beam can be scanned continuously in the elevation plane for the chosen azimuthal direction. 2D LWA with a broadband and a wide-angle scanning range has been proposed in paper [12]. It is composed as a leaky-wave metasurface (MTS) with a four-port feeding located at the structure center. The leaky-wave radiator is divided into four angular sectors, each one devoted to the formation of a beam in a given elevation plane. At a fixed frequency, different azimuthal angle can be obtained if four ports are separately excited. The radiation pattern controlled in azimuth by switching

into particular sectors as presented in paper [12] does not however represent the continuous beam steering.

This paper presents a 2D LWA where the direction of the main lobe radiation pattern in the azimuthal plane is controlled by setting amplitudes of feeding power into two ports at the adjacent antenna matrix edges, a design drawing on the work described in paper [7]. The presented antenna is fed through power dividers designed in substrate-integrated waveguide (SIW) technology. The 2D radiating MTS is composed of mushroom cells coupled by slots in the top surface. The whole structure is therefore designed in an up-to-date compact integrated form, as distinct from paper [7]. The practical feasibility of the concept was thus verified, including the design of a spatially compact version using a resistive termination (antenna B). The novelty of the work is in the compactness antenna structure and in its behavior assuring the continuous steering of the beam in the azimuthal range covering 360°.

The main advantage and the novelty of the antenna array presented here is no need to use phase shifters that naturally consume energy and increase losses. The aim of this work is to specifically show the proof of concept of the LWA with continuous beam steering in the whole azimuthal plane.

The predicted behavior has been verified by experiments.

2D matrix representing an LWA

This paper presents the above-mentioned 2D planar LWA structure, designed unlike in paper [7] in a compact integrated form, which includes eight-port SIW power dividers [13, 14] connected directly to the 2D CRLH mushroom structure [15]. These cells are capacitively coupled to neighboring cells via slots in the top metallization. This structure radiates in the way controlled by the amplitudes of the signal fed to the particular edges of the matrix.

The beam steering in elevation is due to the change in frequency and represents the standard LWA behavior, as will be described by dispersion characteristics, see Fig. 5. The elevation angle θ is measured from axis z, which is perpendicular to the MTS, see Fig. 1.

The beam steering in azimuthal angle is caused by the interaction of two excited internal leaky waves. These waves are quasi-transversal-electromagnetic (TEM) waves with electrical field directed along the z axis, magnetic field is rectangular to the direction of propagation, i.e., parallel to the y axis for the wave with power P_1 and parallel to the x axis for the wave with power P_2. The superposition of these two waves is the leaky wave propagating in the direction φ, see Fig. 1. Angle φ is determined by the direction of the final magnetic field vector. The beam direction in the azimuthal plane is naturally equal to this angle φ and is therefore controlled by changing powers P_1 and P_2 fed into adjacent ports represented by the matrix edges, see Fig. 1, and is determined by [7]

$$tan\,(\varphi) = P_2/P_1. \tag{1}$$

The radiating structure is represented by the 2D matrix of mushroom cells. Following paper [16], the equivalent lumped-element circuit of the rectangular unit cell shown in Fig. 2 is illustrated in Fig. 3. The structure has been analyzed as lossless, so that all included resistors are disregarded.

The elements of the circuit are given by formulas that have been derived based on ideas presented in paper [16]:

$$C_V = \frac{\varepsilon_0\varepsilon_r\,(l^2 - \pi a^2)}{d} \tag{2}$$

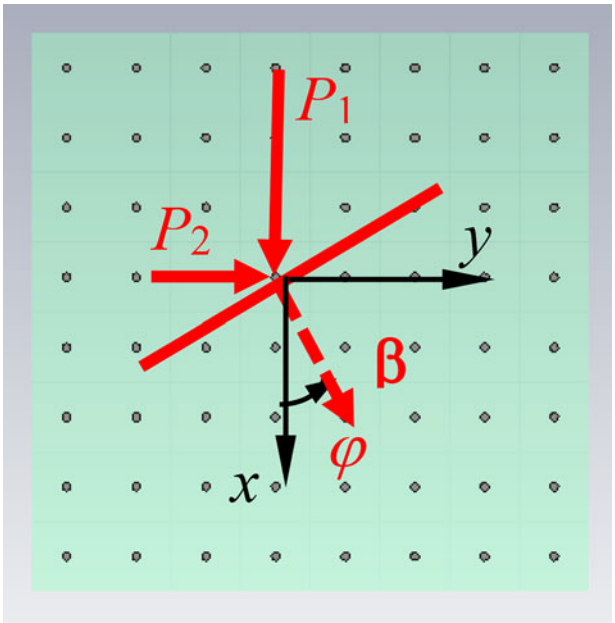

Figure 1. A 2D CRLH transmission line composed of mushroom cells coupled by slots, represents a metasurface. Picture shows the construction of the internal leaky wave propagating under angle φ determined by the propagation vector β.

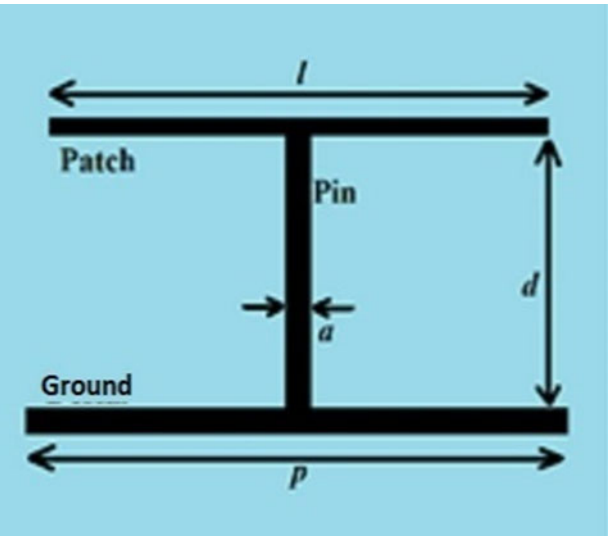

Figure 2. The mushroom cell geometry and dimensions.

$$C_F = \varepsilon_0\varepsilon_r\frac{2p}{\pi}\ln\left(\sin^{-1}\left(\frac{\pi\,(p-l)}{2p}\right)\right) \tag{3}$$

$$L_P = \frac{\mu_0 l_p}{2\pi}\left(\ln\left(\frac{2l_p}{w_p + t_p}\right) + \frac{1}{2}\right) \tag{4}$$

$$L_G = \frac{\mu_0 l_g}{2\pi}\left(\ln\left(\frac{2l_g}{w_g + t_g}\right) + \frac{1}{2}\right) \tag{5}$$

$$L_V = \frac{\mu_0 d}{4\pi}\left(\ln\left(\frac{p^2}{a^2}\right) + \frac{a^2}{p^2} - 1\right) \tag{6}$$

https://doi.org/10.1017/S1759078724000448 Published online by Cambridge University Press

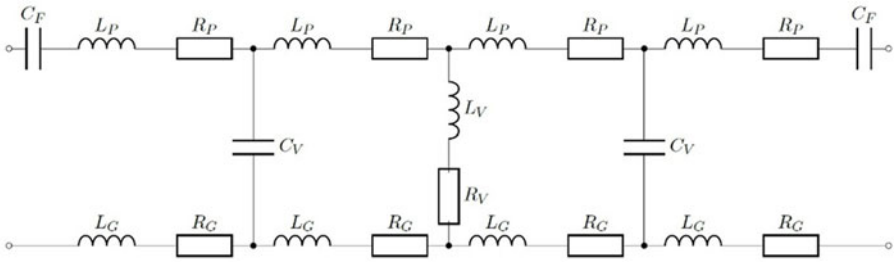

Figure 3. Equivalent lumped-element circuit of the unit cell shown in Figure 2.

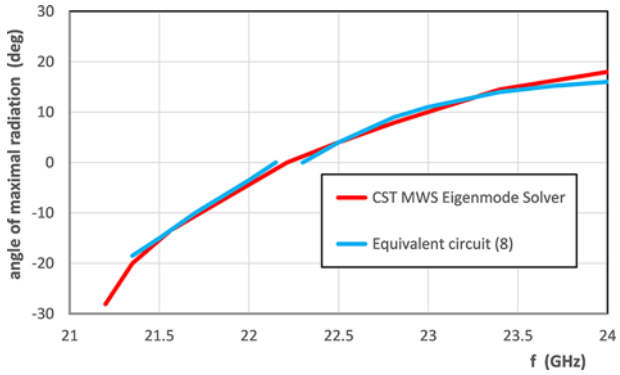

Figure 4. Comparison of the dispersion characteristic calculated by equation (8) with the characteristic calculated by the CST MWS Eigenmode Solver. The phase constant is substituted by the elevation angle by using equation (10).

where l_p, l_g, w_p, w_g are dimensions of the patch and the ground (equal to l, and p in Fig. 2), t_p and t_g are thicknesses of the patch and ground metallization. Next, the ABCD matrix of the circuit in Fig. 3 is determined. The generally complex propagation constant

$$\gamma = \alpha + j\beta \tag{7}$$

where α is the attenuation and β is the phase constant, is given in terms of the ABCD matrix elements as:

$$\gamma = \frac{\operatorname{argcosh}\left(\frac{A+D}{2}\right)}{p}. \tag{8}$$

The characteristic (7) describes the propagation of a wave in the Γ–X direction of the 2D matrix composed of mushroom cells. The dispersion characteristic calculated by equation (8) is compared with the characteristic calculated by the CST Microwave Studio (CST MWS) [17] Eigenmode Solver in Fig. 4. This corresponds to the dispersion characteristic plotted for the designed antenna in Fig. 5.

The Bloch impedance is determined by [18]

$$Z_B = \frac{2B}{(D-A) \pm \sqrt{(A+D)^2 - 4}}. \tag{9}$$

The $\pm$ solutions correspond to the characteristic impedance for positive and negative travelling waves, respectively. For symmetrical networks, these impedances are the same except for the sign; the characteristic impedance for a negatively travelling wave turns out to be negative.

This radiating structure has been designed to show balanced behavior with broadside radiation at 22.25 GHz. At the same time, relatively small cell dimensions have been required. The cells have been designed using a substrate of 0.625 mm in thickness and permittivity equal to 10. The thickness of metallization is 35 μm. The cell dimensions are 5 × 5 mm, the slots between the top metal patches are 0.1 mm in width, and the metallic pins connecting the top patches with the ground are $a = 0.6$ mm in diameter.

The dispersion characteristic of this cell in the first Brillouin zone calculated by the Eigenmode Solver of the CST MWS is plotted in Fig. 5. Instead of the propagation constant β, the plots show the angle of the maximum radiation in elevation θ determined by

$$sin\,(\theta) = \beta / k_o \tag{10}$$

where k_o is the free space propagation constant. These values are plotted in solid lines, where red is for propagation in the Γ–X direction (propagation along the x or y axis) and black for propagation in the Γ–M direction (propagation in the diagonal direction).

Dots in Fig. 5 correspond to elevation angles of maximum radiation according to radiation patterns calculated by the CST MWS. These calculations and measurements were performed by analyzing the whole antenna array, see Fig. 7(b). Equation (10) describes the radiation of an ideal structure organized as an infinite array of individual cells and is not always valid for real structures. This is the reason for the imperfect fit between data in Fig. 5. The plotted dispersion characteristics indicate that the radiation of the 2D antenna matrix is similar in the vicinity of the Γ point (center of the Brillouin zone) both for direction of the wave propagation under 45° (which is the Γ–M direction) and for direction of the wave propagation under 0° or 90° (which is the Γ–X direction). The former refers to the matrix fed from two adjacent ports by equal powers, while the latter corresponds to feeding at only one port. The plot in Fig. 5 confirms that the antenna operates as a 2D CRLH transmission line in balanced regime, i.e., with zero frequency gap. Measurements show that by changing frequency from 21 to 23.8 GHz, the beam is steered in the elevation direction from −20° (backward radiation) to 20° in the forward direction when exciting the antenna at only one port. This interval of angles is reduced to the band from −15° to 15° when exciting the antenna at two ports at equal amplitudes. The dispersion characteristics plotted in Fig. 5 depend on the azimuthal direction of the wave propagation in the structure. From this follows that the radiating patterns defined in the elevation depend on the azimuthal angle. This will be shown in Figs. 14, 16, and 18. The radiation in elevation angles is determined by frequency dependences of the dispersion characteristics.

The leakage constant (real part of the complex propagation constant (7)) is plotted in Fig. 5(b) for the wave propagating at the Γ–X direction, i.e., wave excited by only one port. These values have been calculated by equation (8) as stated in paper [19] using the cell ABCD matrix calculated by the CST MWS analyzing a transmission line that represents a single row or column of the radiating MTS matrix. Three values of the conducting pin radius are used 0.1 mm, 0.3 mm (value applied in the designed antenna), and 0.5 mm. The value of the leakage constant determines the antenna gain. There is an optimum value of the leakage constant to ensure

https://doi.org/10.1017/S1759078724000448 Published online by Cambridge University Press

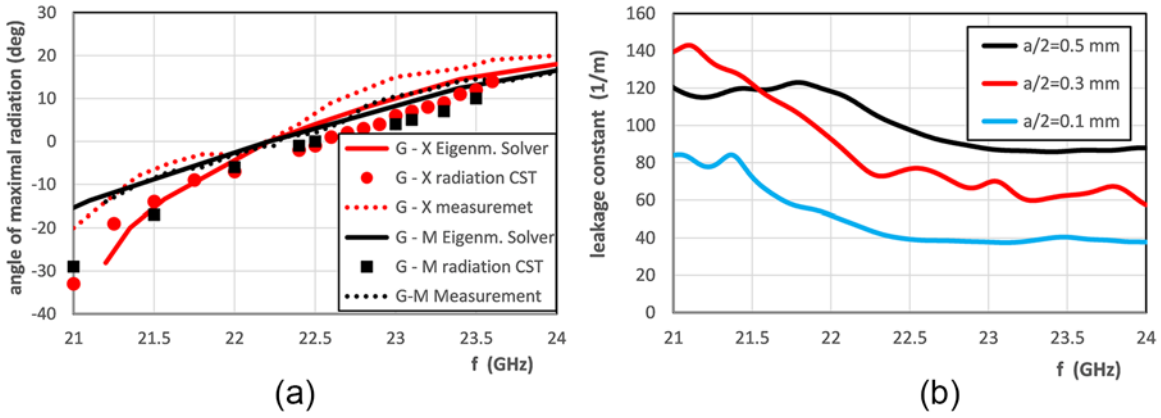

Figure 5. (a) Dispersion characteristics of the 2D antenna matrix calculated by the Eigenmode Solver of the CST MWS are represented by solid lines. Dots correspond to values read from radiation patterns calculated by the CST MWS. Red color represents the wave propagation under an azimuthal angle of 0° (fed at only one port, Γ–X direction). Black color represents the wave propagation under an azimuthal angle of 45° (fed at two adjacent ports, Γ–M direction). (G stands for Γ in the plot legend.) (b) Leakage constant calculated by the CST MWS for the wave propagating at azimuthal angle 0° and for particular pin radii.

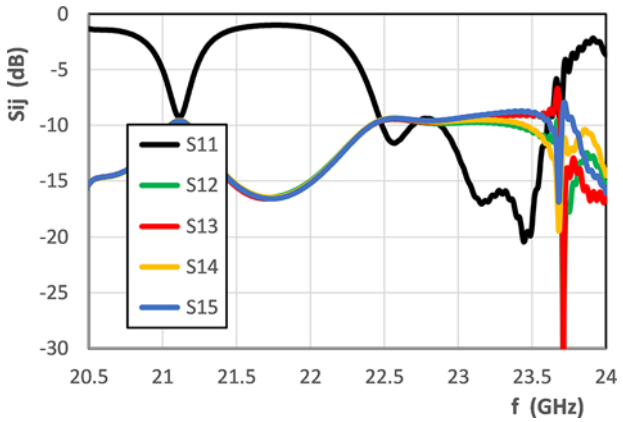

Figure 6. Calculated S_{ij} parameters of the eight-port SIW power divider, where $j = 1$–5, $i = 1$ stands for the feeding 50 Ω microstrip line.

maximal gain. In the case of the proposed antenna, the maximal gain has been obtained for the radius of the conducting pins equal to 0.3 mm, see Fig. 20. The radius equal to 0.5 mm gives substantially lower gain than the radius equal to 0.3 mm. For the radius equal to 0.1 mm, the gain is up to frequency 22.5 GHz nearly the same as for 0.3 mm, for higher frequencies it is lower.

Models of the presented antenna

The radiating structure – 2D matrix of mushroom cells has been discussed and analyzed in the previous paragraph. The matrix composed of 8 × 8 mushroom cells is fed through eight-port SIW power dividers [13, 14] connected directly to the 2D CRLH mushroom structure. The design of the divider has been done according to paper [13]. All SIW parts are of the same width equal to the dimension of the mushroom cell 5 mm. The final calculated scattering parameters are plotted in Fig. 6. The structure is symmetrical therefore only four ports adjacent to the particular cells are considered. The divider behavior is acceptable in the band between 22.5 and 23.5 GHz used in simulations and measurement in following text. This band is the working band of the designed antenna version B, see Fig. 13.

The standard SIW divider structure has been used. The alternative structure is that one presented in paper [20] that occupies less space on the PCB structure.

Two versions of the proposed 2D LWA has been designed and fabricated. The first structure (antenna A) uses four dividers connected to four perpendicular edges of the 2D matrix (see Fig. 7(a)); the second structure (antenna B) uses only two dividers, while the two remaining matrix edges are terminated by resistors ensuring the matching of individual lines (see Fig. 7(b)). Each cell at these edges is terminated by two resistors connected in parallel. The antenna A structure enables steering the beam in dependence on feeding from particular ports in the azimuthal plane in the whole interval of 360°. In contrast, the simplified antenna B structure provides beam steering only within 90°. However, as will be shown later, the constructed specimen A shows worse symmetry compared to the constructed specimen B. The problem is in the imperfect fabrication of the power dividers in antenna A. Specimen B utilizes power dividers with improved behavior.

The resistors terminating the edges of the individual mushroom cells have values of 30 Ω. So the termination of these edges is 15 Ω. This corresponds to the Bloch impedance of the mushroom arrays forming the individual rows and columns of the matrix. These impedances were calculated from the ABCD matrix by formula (9). The resistors do not significantly reduce the efficiency of the antenna because the field at the respective edges is due to the leakage relatively weak as the transmission of particular rows and or columns (S_{21}) of the radiating metamaterial matrix are in the whole frequency band lower than 0.09. This was calculated by the CST MWS and corresponds to the value of the leakage constant from Fig. 5(b). This S_{21} can be reduced by increasing a radius of used pins in mushroom cells or by reducing the width of slots between cells. These changes in the cell structure however would detune the dispersion characteristic – frequency of broadside radiation and the band of the antenna matching.

Beam steering in the azimuthal plane is documented in Fig. 8, which shows the simulated distribution of electric field excited by antenna B, depending on the power fed into particular ports. The plots represent radiation patterns calculated by the CST MWS in the Cartesian coordinate system at the 23.4 GHz frequency, offering radiation in the forward direction. The relative feeding amplitudes applied in particular plots in Fig. 8 are as

https://doi.org/10.1017/S1759078724000448 Published online by Cambridge University Press

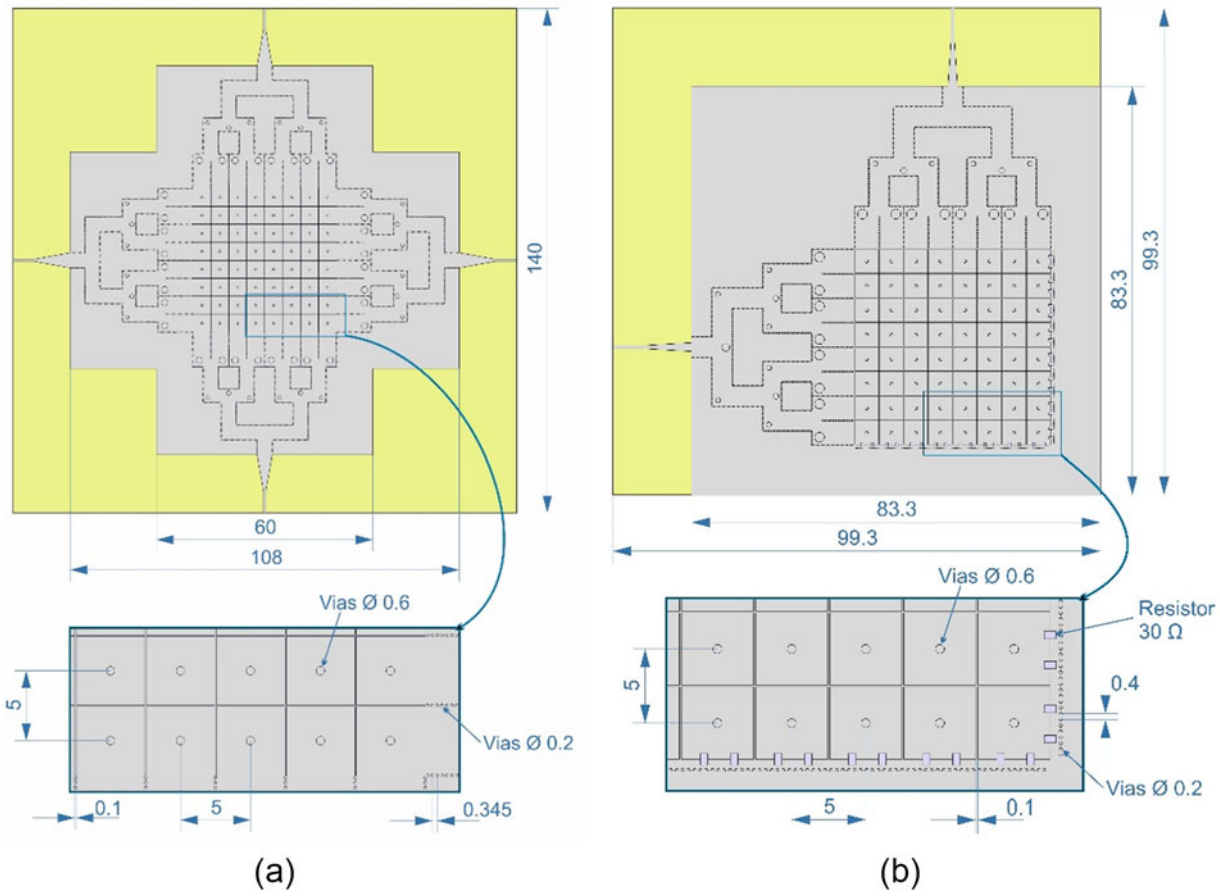

Figure 7. Sketch of the 2D antenna matrix. (a) Antenna A is fed by the power dividers at all four ports. (b) Antenna B is fed only at two orthogonal ports. The antenna matrix is terminated by lumped resistors (two in parallel to each individual cell) at the remaining edges. Dimensions are in mm.

follows: (a) [1, 0], (b) [1, 0.414], (c) [1, 0.708], (d) [1, 1], (e) [0.708, 1], (f) [0.414, 1], and (g) [0, 1]. According to equation (1), the azimuthal angles correspond to 0°, 22.5°, 35.5°, 45°, 54.5°, 67.5°, and 90°. Fig. 8 clearly shows the rotation of the beam main lobe in the azimuthal plane within 90°. The radiation beam is widened when moved to the oblique direction as the antenna is fed by two waves. The beam is even wider at frequency 24 GHz at which the elevation angle is higher, see Fig. 5, than shown in Fig. 8(d). This is due to the superposition of the two particular beams that have maxima at greater distance.

The radiated field has a linear polarization. The electric field vector direction is parallel to the vector β defined in Fig. 1.

Measurement of 3D radiation patterns

The antenna matrix is generally excited at two ports supplying different power at the same phase. The measurement setup is presented in Fig. 9.

The 3D radiation patterns of the antenna under test (AUT) have been obtained in a fully anechoic chamber. It is equipped with a roll-over-azimuth measuring system, where the AUT is mounted on the roll (φ) positioner, which is in turn attached to the elevation (θ) positioner. The AUT is scanned in a 200° azimuthal span ($\pm$100°) with a 1° step for the whole 180° φ range to obtain hemispherical radiation patterns. At each measured point, the receiving probe antenna (DRH40 [21]) is rotated to both orthogonal (0° and 90°) positions to obtain precise polarization information from the AUT. The AUT and the probe antenna are separated by a distance of 4 m.

Antenna patterns are measured and computed automatically, employing the NSI2000 far-field measuring software [22] for a predefined frequency span. The measuring system uses the two-port vector network analyzer (VNA) Rohde & Schwarz ZVA40 as a transmitter/receiver. In this setup, the AUT is connected to one port of the VNA, the test probe to the second one, and the S_{21} transmission coefficient is measured. The gain was determined by the gain-transfer method using the antenna with known gain – DRH40 [21]. The antenna feeding is implemented by means of a two-way power divider (Pulsar PS2-50-450/8S [23]) with a very low phase imbalance (below 6°) and amplitude imbalance (below 0.5 dB). The antenna is connected to the divider by cables with identical (electrical) length. The appropriate amplitude difference at port 1 and port 2 is ensured by an attenuator attached to one port of the AUT, while on the second port, an adapter with same electric length as the used attenuator is mounted.

Experimental verification

Antenna A

The constructed 2D antenna matrix, version A, is shown in Fig. 10. Two ports are connected to a network analyzer, the remaining two are matched. The calculated and measured scattering parameter S_{ii} is plotted in Fig. 11 for $i = 1–4$. The drawback of the

https://doi.org/10.1017/S1759078724000448 Published online by Cambridge University Press

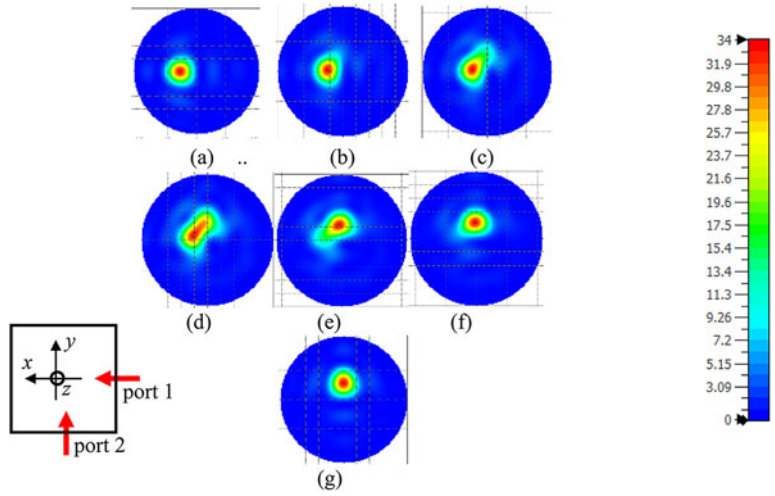

Figure 8. Radiation patterns (directivity normalized to the same maximum, see the scale) of the version B antenna matrix for particular feeding conditions into two ports calculated by the CST MWS at 23.4 GHz. The given antenna ports are fed by the following amplitudes: (a) [1, 0], (b) [1, 0.414], (c) [1, 0.708], (d) [1, 1], (e) [0.708, 1], (f) [0.414, 1], and (g) [0, 1]. The inset shows the position of feeding ports valid for these plots together with the coordinate system.

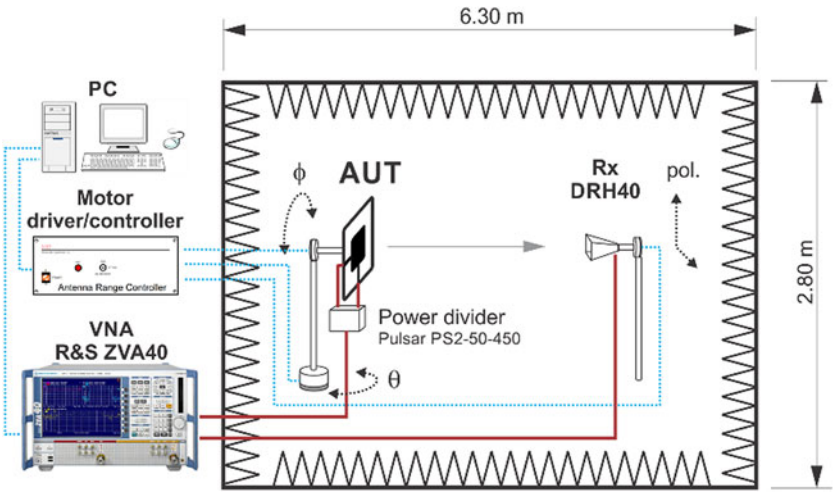

Figure 9. The 3D radiation pattern measurement setup.

version A antenna is its lack of symmetry, caused by power dividers that are not identical. The reason for this shortcoming is the imperfect technology process, consisting in drilled holes for SIW sidewall pins. The antenna is well matched around 23.4 GHz. The version A antenna has the same results in simulations of radiated fields as the version B antenna. Therefore, all experiments have been conducted by using the version B antenna (see the next paragraph).

Antenna B

The constructed 2D antenna matrix in version B is shown in Fig. 12. A comparison of the S_{11} parameter as measured and as simulated by the CST MWS for the antenna matrix B is provided in Fig. 13. The measurement shows the band of proper antenna behavior, where $S_{11} < -10$ dB between 22.3 and 23.4 GHz.

Fig. 14 shows the evolution of the 3D radiation pattern of the antenna matrix B measured at 23.4 GHz. The antenna is fed from two ports with equal amplitudes of [1, 1]. Individual lines in Fig. 14 are measured at increasing elevation angles, starting from 12° up to 20°, measured from the broadside direction. They represent the radiation pattern measured on a sphere as a function of the azimuthal angle φ taken between 0° and 90°. This evolution corresponds to the 2D radiation pattern from Fig. 8(d). The maximum of the radiation is at 45°, as expected.

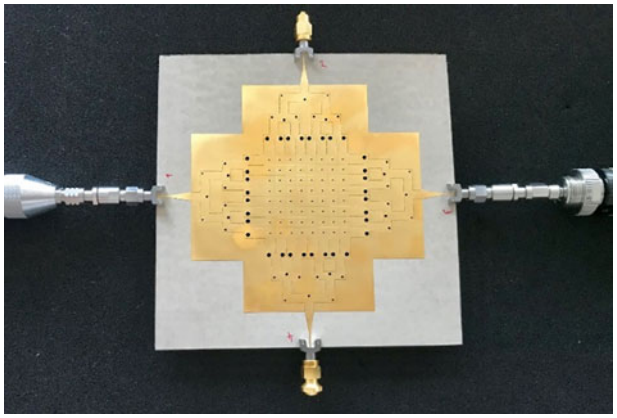

Figure 10. The constructed antenna matrix, version A.

A comparison of radiation patterns of the antenna matrix B as measured and as simulated by the CST MWS is provided in Fig. 15. The frequency used is 23.4 GHz and the patterns are taken at the 45° azimuthal angle. The antenna is fed by equal powers into its two ports. The measurement corresponds to the simulation, apart from the sharp dip measured at 6°.

https://doi.org/10.1017/S1759078724000448 Published online by Cambridge University Press

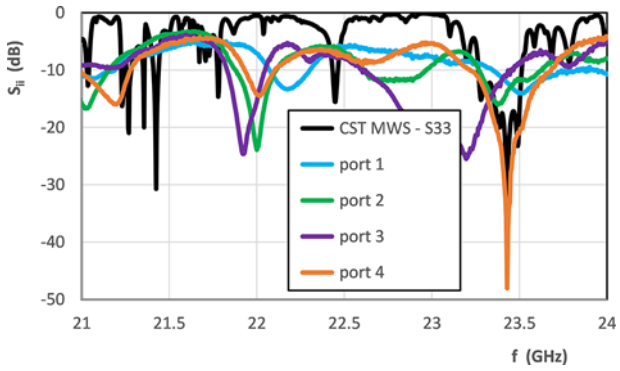

Figure 11. Comparison of measured and calculated (black line) S_{ii}, antenna matrix version A.

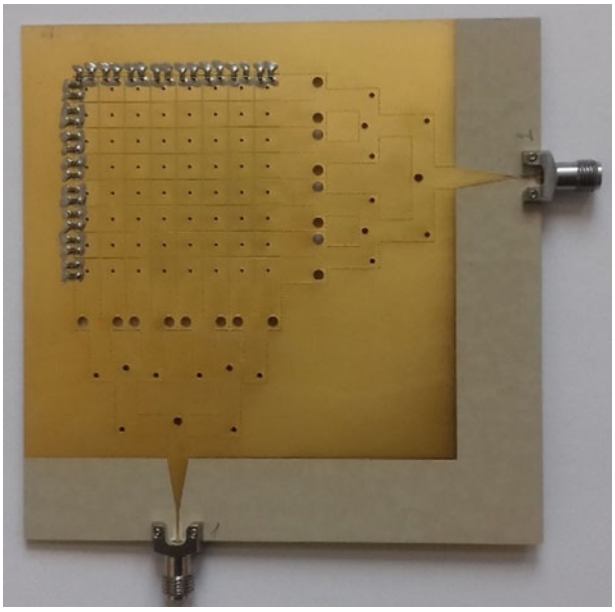

Figure 12. The constructed antenna matrix, version B.

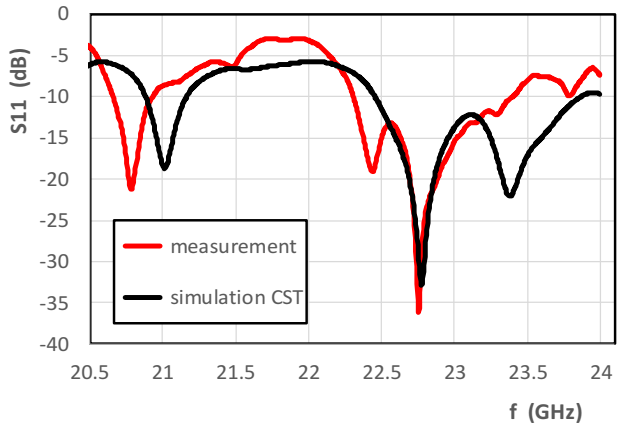

Figure 13. Comparison of the measured and calculated S_{11} parameter, antenna matrix version B.

The next experiment has been performed by attaching the −3 dB attenuator into the P1 port, so the antenna is now fed from two ports with amplitudes of [0.708, 1]. Here the azimuthal angle of the maximum radiation according to equation (1) is $\varphi = 54.5°$. The evolution of the measured radiation pattern at a feeding of [0.708, 1] with an increasing elevation angel is plotted in Fig. 16. The maxima of the individual patterns correspond to an azimuthal angle of 54.5°. The maximum of the radiation is between elevation angles 12° and 24°. This measured field distribution corresponds to the 2D radiation pattern from Fig. 8(e).

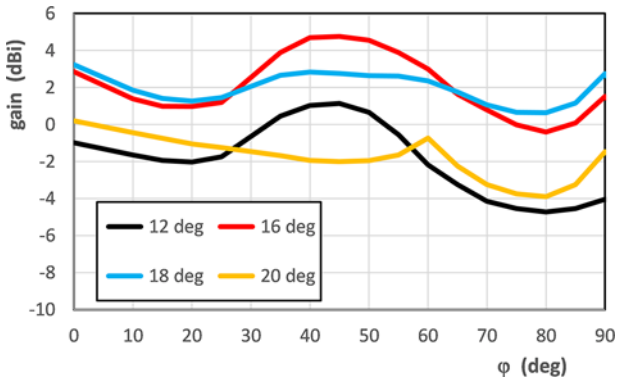

Figure 14. Details of 3D radiation patterns measured at 23.4 GHz and at given elevation angles θ varying from 12° up to 20°. The antenna is fed from two ports with equal amplitudes [1, 1].

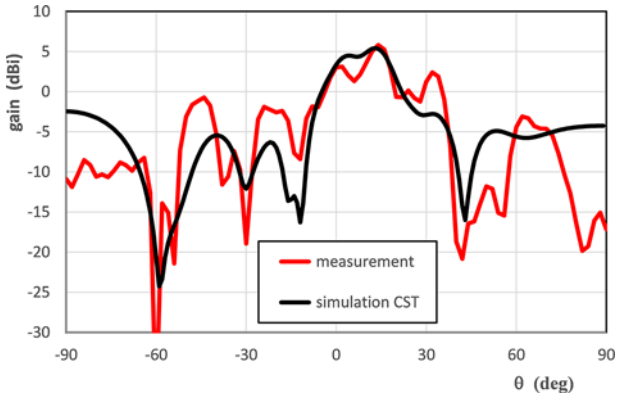

Figure 15. Measured and simulated radiation patterns of the antenna matrix version B at 23.4 GHz as a function of the elevation angle θ at an azimuthal direction of 45°. The antenna is fed from two ports with equal amplitudes.

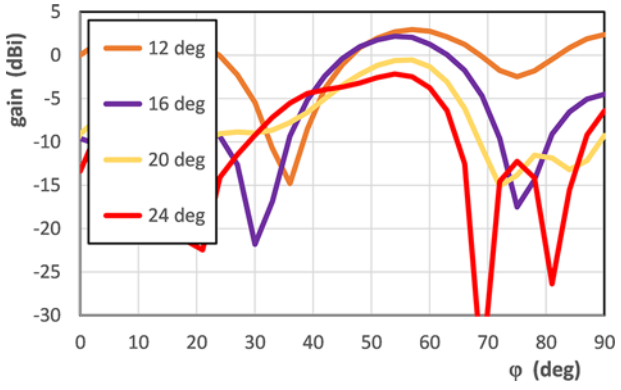

Figure 16. Details of 3D radiation patterns measured at 23.4 GHz and at given elevation angles θ varying from 12° up to 24°. The antenna is fed from two ports with amplitudes of [0.708, 1].

https://doi.org/10.1017/S1759078724000448 Published online by Cambridge University Press

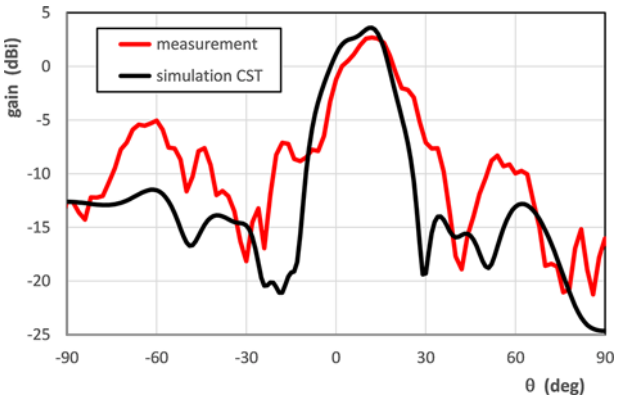

Figure 17. Measured and simulated radiation patterns of the antenna matrix version B at 23.4 GHz as a function of the elevation angle θ at an azimuthal direction of 54.5°. The antenna is fed from two ports with amplitudes of [0.708, 1].

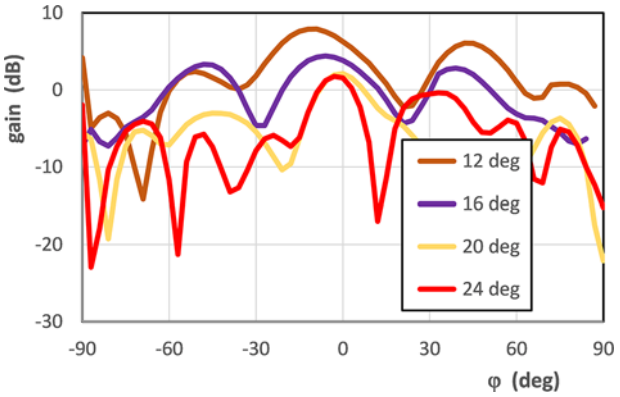

Figure 18. Details of 3D radiation patterns measured at 23.4 GHz and at given elevation angles θ varying from 12° up to 24°. The antenna is fed from one port.

A comparison of radiation patterns as measured and as simulated by the CST MWS for the antenna matrix B is provided in Fig. 17. The frequency used is 23.4 GHz and the patterns are taken at an azimuthal angle of 54.5°. The antenna is fed from two ports with amplitudes of [0.708, 1].

The final experiment has been performed by feeding the antenna from only one port, i.e., [1, 0]. Here the azimuthal angle of maximum radiation is naturally 0°. The evolution of the measured radiation pattern with an increasing elevation angel is plotted in Fig. 18. The maxima of individual patterns oscillate around an azimuthal angle of 0°. The maximum of the radiation at elevation is at around 20°. This evolution corresponds to the calculated 2D radiation pattern from Fig. 8(g).

A comparison of radiation patterns as measured and as simulated by the CST MWS for the antenna matrix B is provided in Fig. 19. The frequency used is 23.4 GHz and the patterns are taken at an azimuthal angle of 0°. The antenna is fed from one port. The measurement corresponds to the simulation, apart from the wavy character of the measured pattern.

Plots in Figs. 14, 16, and 18 verify the capability to steer the beam by changing amplitudes of signals feeding the specific antenna matrix ports as predicted theoretically in Fig. 8 and according to equation (10).

Fig. 20 plots measured and calculated gain in the broadside direction versus frequency. The measured data fit sufficiently the data simulated by CST. Fig. 21 plots the gain measured at 22.45 and

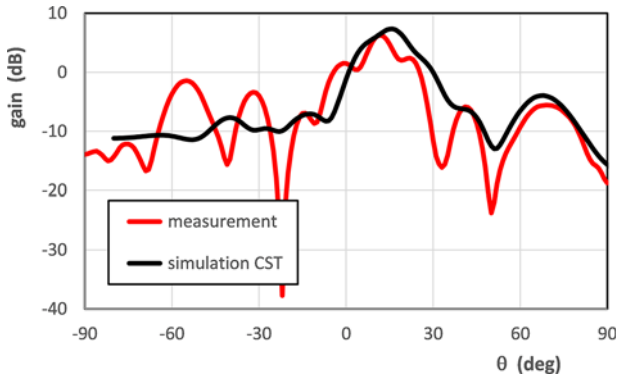

Figure 19. Measured and simulated radiation patterns of the antenna matrix version B at 23.4 GHz as a function of the elevation angle θ at an azimuthal direction of 0°. The antenna is fed from one port.

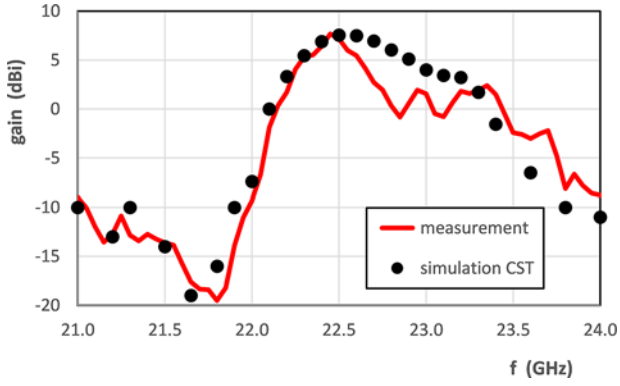

Figure 20. Measured and simulated antenna gain at the broadside direction as the function of frequency. The antenna is fed from one port [1, 0].

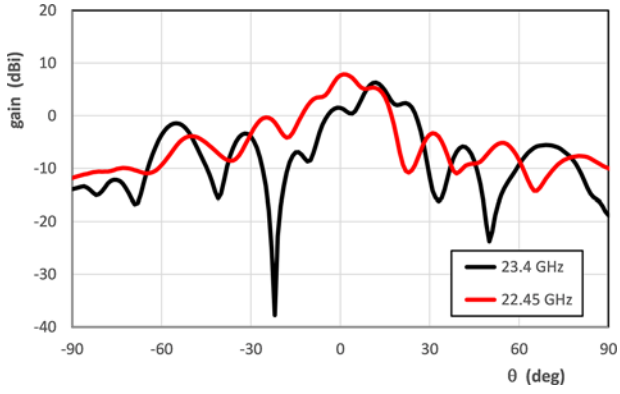

Figure 21. Measured antenna gain at frequencies 22.45 and 23.4 GHz at an azimuthal direction of 0° as the function of the elevation angle. The antenna is fed from one port [1, 0].

23.4 GHz as a function of elevation angle, taken at an azimuthal angle equal to 0°. The antenna was in these two measurements excited from only one port, i.e., excitation [1, 0], as in Figs. 18 and 19. The radiation pattern plotted in Fig. 21 at frequency 23.4 GHz copies, except the scale, the patterns plotted in Fig. 19. Figure 21 shows as well the gain measured at frequency 22.45 GHz, where Fig. 20 shows the maximal value that is about 7 dBi.

The maximum antenna gain is approximately 7 dBi for the antenna fed to one port at frequency 22.45 GHz, see Fig. 21.

https://doi.org/10.1017/S1759078724000448 Published online by Cambridge University Press

Table 1. Comparison of the proposed design and other 2D leaky-wave antennas (according [24])

	[11]	[12]	[24]	[25]	[26]	[27]	[28]	[29]	This work Antenna B
Antenna type	Fabry–Perot cavity	2D MTS	2D planar SWL LWA	Annular strip gratings	2D slot array	2D CTSs slots	2D periodic	2D matrix	2D LW matrix – MTS
Guiding structure	MTS	LW MTS	Grounded dielectric slab	Radial WG	Meandered rectangular WG	Parallel-plate WG	Wedge-like WG	SIW	2D grounded mushroom cells
Maximum gain frequency (GHz)	5.5	10.5	19.48	18	237.5	42	32	25.2	22.25
Gain (dBi)	15.3	12.29	18.6	–	28.5	29.2	20.3	24.9	7
Total efficiency (%)	13	32	57	57–97	55–56	63–89	88–91	76	35
SLL (dB) *E*-plane	−10	−7	−10	−4 to −8	−10.9	−12.6 to −16	−10.6 to −19	−10	−11
SLL (dB) *H*-plane	−12	−9	−5	–	−12.5 to −13.3	–	−5	−10	–
Grating/back lobe (dB)	–	−10	–	−22	−10	–	−14.7	–	–
Impedance BW (%)	–	30	20.5	40	6.3	38	24.4	2.8	4.9
3-dB gain BW (%)	–	–	5.1	–	6.3	24	15	2.4	4.9
Relative size (λ_0^2)	5.4 × 5.4	6.51 × 6.51	6.6 × 6.6	2 × π × 16.8	35.6 × 6.7	18.6 × 13	8.16 × 8.43	13.1 × 13.1	3 × 3
Scanning ability (degrees), way of scanning	30 elevation varactors 4 sectors in azimuth	75 elevation freq. 4 sectors in azimuth	17, freq. elevation	–	50, freq. azimuth	54, freq. elevation	28, freq. elevation	36, freq. elevation	40, freq. elevation 90, controlled by feeding ampl., azimuth

The radiation efficiency of the antenna estimated from the simulation performed by CST MWS is approximately 35%. The relatively low gain and efficiency values are due to losses in the power dividers used. The other reason of the low gain is in the relatively small radiating area of the presented structure that is the matrix of 8 × 8 mushroom cells of dimensions 5 × 5 mm, i.e., 40 × 40 mm, that is 3 × 3 λ_o at frequency of the maximum gain 22.25 GHz, see Fig. 7(b). This dimension is shown in Table 1.

Table 1 compares the parameters of the presented antenna with data taken from the literature. The antenna array presented in paper [7] is able to steer the beam in the azimuthal plane as well as our design. The paper [7] did not present any parameters shown in Table 1. The paper [7] only proposed the idea. The same is valid for paper [10]. For all the antennas listed in Table 1, the beam steering in elevation is controlled by changing the frequency. That is not the case of paper [11] where the direction of the main beam in elevation is controlled by DC voltage setting varactors capacities. Our goal was to present a reconfigurable antenna with a radiation pattern controlled by external means, in this case by feeding the structure into individual ports with variable amplitude, not by changing the frequency, which is the feature of standard LWAs. The radiation pattern controlled in azimuth by switching into particular sectors as presented in paper [12] does not however represent the continuous beam steering.

The measured side lobe level (SLL) of the antenna is around −5 dB in most of the presented results. The maximum difference of the side lobe from the main lobe was experimentally obtained around −11 dB, as shown in Fig. 16 at the elevation angle 20° (experiment performed with the attenuator inserted in port P1 – feed [0,708, 1]). The simulation shows the best SLL value of −13.5 dB for an antenna fed only to one edge – feed [1, 0]. The antenna radiation efficiency (simulated) is quite small, approximately 35%. This is due to losses in the power dividers.

Conclusion

The paper presents a 2D MTS LWA array. This antenna has been designed using an up-to-date integration version of SIW technology, including power dividers feeding the specific ports of the matrix composed of mushroom cells. Therefore, the structure is fully compact. The direction of the antenna maximum radiation can be steered in azimuthal angle by changing amplitudes of the signal feeding the particular antenna ports. The main advantage of the presented antenna is no need to use phase shifters increasing losses of the antenna. Two antenna versions have been designed, fabricated, and experimentally tested. Version A is fed by four power dividers and enables the continuous beam steering in a total interval of azimuthal angles equal to 360°. Version B is fed by two power dividers into two adjacent matrix edges, while the other two edges are terminated by resistors. This antenna structure enables the continuous beam steering in only one quadrant, i.e., in a range of 90°. The drawback of the constructed antenna in version A is its lack of symmetry, caused by power dividers feeding individual matrix edges that are not identical due to the nonperfect fabrication process.

By changing frequency from 21 to 23.8 GHz, the antenna beam can be steered in the elevation direction from −20° (backward radiation) to 20° in the forward direction when exciting the antenna from only one port. This interval of angles is reduced to the band from −15° to 15° when exciting the antenna from two ports at equal amplitudes. This provides the limitation of the beam steering that is caused by the radiating structure dispersion. Due to this, the radiation patterns in elevation depend on the azimuthal angle.

The performed experiments verified the antenna behavior presented by simulation, namely, continuous beam steering in the azimuthal direction.

Acknowledgements. This work was supported partly by the Czech Science Foundation (project no. 20-02046S), partly by the Ministry of Education, Youth and Sports of the Czech Republic (program INTER-EXCELLENCE, subprogram INTER-COST, project LTC20012), and by COST – European Cooperation in Science and Technology (COST Action CA18223 – SyMat).

Competing interests. The author(s) declare none.

References

1. **Sanada A, Caloz C and Itoh T** (2004) Planar distributed structures with negative refractive index. *IEEE Transactions on Microwave Theory & Techniques* **52**(4), 1252–1263.
2. **Sarkar A, Sharma A, Biswas A and Akhtar MJ** (2019) EMSIW-based compact high gain wide full space scanning LWA with improved broadside radiation profile. *IEEE Transactions on Antennas and Propagation* **67**(8), 5652–5657.
3. **Allen CA, Caloz C and Itoh T** (2004) Leaky-waves in a metamaterial-based two-dimensional structure for a conical beam antenna application. In *2004 IEEE MTT-S International Microwave Symposium Digest*, T 1D-2, 1, 305–308.
4. **Podilchak SK, Freundorfer AP and Antar YMM** (2008) Planar leaky-wave antenna designs offering conical-sector beam scanning and broadside radiation using surface-wave launchers. *IEEE Antennas and Wireless Propagation Letters* **7**, 155–158.
5. **Ren D, Li Z, Choi JH and Wu R** (2020) 1D & 2D W-band frequency scanning metamaterial antenna and array. In *2020 IEEE International Symposium on Antennas and Propagation and North American Radio Science Meeting*, 171–172.
6. **Jackson DR, Capolino F, Almutawa A, Kazemi H, Sengupta S, Fuscaldo W, Galli A and Long SA** (2020) Review of recent advances in the leaky-wave analysis of 2-D leaky-wave antennas. In *14th European Conference on Antennas and Propagation (EuCAP)*.
7. **Lai A, Leong KMKH and Itoh T** (2006) Leaky-wave steering in a two-dimensional metamaterial structure using wave interaction excitation. In *2006 IEEE MTT-S International Microwave Symposium Digest*, 1646–1646.
8. **Ashtiani F and Aflatouni F** (2020) Optical beam steering using an N×N phased array with 2N phase shifters. In *2020 Conference on Lasers and Electro-Optics (CLEO)*, San Jose, CA, USA, 1–2.
9. **Dorrah AH and Eleftheriades GV** (2021) Experimental demonstration of peripherally-excited antenna arrays. *Nature Communications* **12**, 6109.
10. **Nguyen HV, Abielmona S, Rennings A and Caloz C** (2007) Pencil-beam full-space scanning 2D CRLH leaky-wave antenna array. In *2007 International Symposium on Signals, Systems and Electronics*, Montreal, QC, Canada, 139–142.
11. **Guzmán-Quirós R, Weily AR, Gómez-Tornero JL and Guo YJ** (2016) A Fabry–Pérot antenna with two-dimensional electronic beam scanning. *IEEE Transactions on Antennas and Propagation* **64**(4), 1536–1541.
12. **Zhang Z, Zhang W, Liu Y, Ma R, Yang R and Han L** (2022) Two-dimensional broadband and wide angle scanning multi-beam antenna based on leaky-wave metasurface. *The International Journal of RF and Microwave Computer-Aided Engineering* **32**(1), e22922.
13. **Hao ZC, Hong W, Li H, Zhang H and Wu K** (2005) Multiway broadband substrate integrated waveguide (SIW) power divider. In *2005 IEEE Antennas and Propagation Society International Symposium*, 1A.
14. **Shehab SH, Karmakar NC and Walker J** (2020) Substrate-integrated waveguide power dividers. In *IEEE Antennas and Propagation Magazine*, 27–38.

https://doi.org/10.1017/S1759078724000448 Published online by Cambridge University Press

15. **Sievenpiper D, Zhang L and Yablonovitch E** (1999) High-impedance electromagnetic ground planes, *1999 IEEE MTT-S International Microwave Symposium Digest*, 4.
16. **Yang X-L, Zhang L, Li Y-S, Jin H, Cheng P, Li Y and Li E-P** (2018) A novel package lid using mushroom-type EBG structures for unintentional radiation mitigation. *IEEE Transactions on Electromagnetic Compatibility* **60**(6), 1882–1888.
17. **Dassault Systemes** (2002) CST Microwave Studio. https://www.3ds.com/products-services/simulia/products/cst-studio-suite
18. **Sabah C, Urbani F and Uckun S** (2007) Frequency dependence of Bloch impedance in left-handed transmission line. In *The Second European Conference on Antennas and Propagation, EuCAP*.
19. **Machac J, Polivka M and Zemlyakov K** (2013) A dual band leaky wave antenna on a CRLH substrate integrated waveguide. *IEEE Transactions on Antennas and Propagation* **61**(7), 3876–3879.
20. **Gómez-Guillamón Buendía V, Podilchak SK, Comite D, Baccarelli P, Burghignoli P, Gomez Tornero JL and Goussetis G** (2019) Compact leaky SIW feeder offering TEM parallel plate waveguide launching. *IEEE Access* **7**, 13373–13382.
21. **RF Spin** (2024) DRH40: Double ridged waveguide horn. https://www.rfspin.com/product/drh40/
22. **NSI-MI Technologies** (2023) https://www.nsi-mi.com/
23. **Pulsar Microwave Corporation** (2024) https://www.pulsarmicrowave.com/product/power_divider/PS2-50-450-8S
24. **Podilchak SK, Freundorfer AP and Antar YMM** (2008) Broadside radiation from a planar 2-D leaky-wave antenna by practical surface-wave launching. *IEEE Antennas and Wireless Propagation Letters* **7**, 517–520.
25. **Comite D, Fuscaldo W, Podilchak SK, Re PD, Buendía VG, Burghignoli P, Baccarelli P and Galli A** (2018) Radially periodic leaky-wave antenna for Bessel beam generation over a wide-frequency range. *IEEE Transactions on Antennas and Propagation* **66**(6), 2828–2843.
26. **Sarabandi K, Jam A, Vahidpour M and East J** (2018) A novel frequency beam-steering antenna array for submillimeter-wave applications. *IEEE Transactions on Terahertz Science and Technology* **8**(6), 654–665.
27. **You Y, Lu Y, You Q, Wang Y, Huang J and Lancaster MJ** (2018) Millimeter-wave high-gain frequency-scanned antenna based on waveguide continuous transverse stubs. *IEEE Transactions on Antennas and Propagation* **66**(11), 6370–6375.
28. **Attar A and Sebak AR** (2020) High gain periodic 2-D leaky-wave antenna with backward radiation for millimeter-wave band. *IEEE Open Journal of Antennas and Propagation* **2**, 49–61.
29. **Yang Q, Gao S, Luo Q, Wen L, Ban YL, Yang X, Ren X and Wu J** (2020) Dual-polarized crossed slot array antenna designed on a single laminate for millimeter-wave applications. *IEEE Transactions on Antennas and Propagation* **68**(5), 4120–4125.

Jan Machac is currently a Professor with the Department of Electromagnetic Field, Faculty of Electrical Engineering, Czech Technical University in Prague, Czech Republic. He is the author or a co-author of more than 250 publications in scientific journals and scientific international and national conferences. His main scientific interests include planar passive elements and subsystems of microwave technology, planar antennas, and microwave filters, propagation of electromagnetic waves in periodic, and artificial electromagnetic structures, chipless RFID, and power wireless transport.

Milan Svanda received the M.S. and Ph.D. degrees in radioelectronics from Czech Technical University in Prague, in 2007 and 2011, respectively. He is currently a Research Scientist with CTU in Prague. He is the author or a co-author of more than 60 articles published in international journals or conference proceedings and co-author of seven patents. His main research activities are focused on antennas operating in close proximity to the human body, low-profile, and wearable RFID and sensor antennas.

Vaclav Kabourek was born in 1985. He received his M.Sc. and Ph. D. degree from the Czech Technical University in Prague in 2010 and 2017. His research interests include antenna design and measurement, RCS measurement. His contemporary research activities are also focused on EMC measurements.

https://doi.org/10.1017/S1759078724000448 Published online by Cambridge University Press